Dyes and Pigments 222 (2024) 111907

Contents lists available at ScienceDirect

Dyes and Pigments

journal homepage: www.elsevier.com/locate/dyepig

Bridge-induced taming of the visible electronic circular dichroism signatures of *helico*BODIPYs

Carolina Díaz-Norambuena [a,b], Cesar Ray [b], Teresa Arbeloa [a], Ainhoa Oliden-Sánchez [a], Florencio Moreno [b], Beatriz L. Maroto [b], Jorge Bañuelos [a,*], Santiago de la Moya [b,**]

[a] Departamento de Química Física. Facultad de Ciencia y Tecnología. Universidad del País Vasco-EHU. Apartado 644, 48080, Bilbao, Spain
[b] Departamento de Química Orgánica. Facultad de Ciencias Químicas. Universidad Complutense de Madrid. Ciudad Universitaria s/n, 28040, Madrid, Spain

ARTICLE INFO

Keywords:
BODIPYs
Dye chemistry
Chirality
Charge transfer
Circular dichroism

ABSTRACT

Helically-flexible bis(BODIPY)s based on chiral ethane-1,2-diamine or −1,2-diol bridges (named *helico*BODIPYs) are an interesting family of accessible and tunable small multichromophoric organic dyes enabling visible electronic circular dichroism (ECD) and, even visible circularly polarized luminescence (CPL). However, their CPL brightness (B_{CPL}) is still limited (up to *ca.* 10 $M^{-1}cm^{-1}$), due to low fluorescence efficiency owing to a non-optimal participation of intramolecular charge transfer (CT) emission. Herein, we analyze in depth the origin and factors controlling this CT, demonstrating the key participation of a BODIPY-to-BODIPY symmetry-breaking induced CT (SBCT), beyond the expected CT within each single BODIPY chromophore due to their push-pull character. It is also demonstrated that increasing the overcrowding at the flexible *helico*BODIPY ethane bridges leads to BODIPY-BODIPY faced dispositions, promoting the SBCT and enabling the detection of both CT absorption and CT emission bands under specific conditions. Interestingly, this SBCT enhances the visible ECD (absolute g_{abs} values), supporting the key role of the involved forbidden CT transitions in the chiroptical activity of these dyes, as well as the possibility of modulating their valuable visible chiroptical signatures (*e.g.*, visible CPL brightness) by easily playing with steric factors at the dye bridge.

1. Introduction

Chirality is a ubiquitous phenomenon that has witnessed a renewed interest in the last years, being a hot topic in Life and Universe Sciences nowadays. Most biomolecules are chiral, and the interaction between drugs and molecules markedly depends on the involved enantiomers. This pivotal role of chirality in many biochemical events has boosted the synthesis of enantioenriched chiral compounds and materials, as well as the design of novel approaches to induce and detect their associated optical activity. In this context, photophysics [1,2] in combination with dye chemistry [3–5] have succeeded in developing advanced molecular systems able to efficiently absorb and/or emit circularly polarized (CP) light. These CP-active molecules, and materials based on them, are of great interest due to their huge potential in a plethora of light-triggered applications. In this context, CP-active materials based on small organic molecules (SOMs) are qualified as next-generation photonic materials [6], owing to their low density (ultralight materials), easy processing, high biocompatibility and cell-membranes permeability, high light absorption and fluorescence response, and easy tunability by workable organic chemistry. Accordingly, different approaches have been reported to successfully design and synthesize SOMs displaying efficient electronic circular dichroism (ECD) and, which is more important and challenging, efficient circularly polarized luminescence (CPL), mainly within the valuable visible spectral region [7–10]. These phenomena involve different ways of interaction with CP light. Thus, ECS is the differential absorption of left- and right-handed CP light, and it is quantified by the corresponding absorption dissymmetry factor (g_{abs}), whereas circularly polarized luminescence (CPL) is the differential emission of left- and right-handed CP light, being quantified by the corresponding luminescence dissymmetry factor (g_{lum}).

However, the development of improved CP-active SOMs, with large absolute g_{abs} and g_{lum} values (higher than 10^{-3}), is still challenging. On the one hand, their molecular size is much smaller than the helical pitch of the visible circularly polarized light, which avoids dichroic

* Corresponding author.
** Corresponding author.
E-mail addresses: jorge.banuelos@ehu.es (J. Bañuelos), santmoya@ucm.es (S. Moya).

https://doi.org/10.1016/j.dyepig.2023.111907
Received 10 October 2023; Received in revised form 4 December 2023; Accepted 20 December 2023
Available online 23 December 2023

amplification effects by birefringence effects [6]. On the other hand, their absorption and emission involve allowed electronic transitions (*i.e.,* with large absolute electric-dipole transition moments, $|\mu|$, but with small magnetic ones, $|m|$). This has the advantage of yielding high absorption and fluorescence efficiencies, but it is a serious limitation for the improvement of the CP activity (note that $g \approx 4\cos\theta|m|/|\mu|$ [11], where θ is the angle formed by the involved moments), and mainly in that concerning CPL that requires also high emission quantum yields (φ) to reach profitable CPL brightness B_{CPL} ($B_{CPL} = \varepsilon\ \varphi\ |g_{lum}|/2$, where ε is the molar absorptivity) [12]. In this context, different strategies are currently being used to design SOMs with improved g_{abs} and g_{lum}, and B_{CPL} values, as well as to understand the complex relationship between the molecular structure and these dichroic values, including their signs [13–17]. Among the approaches towards improving the g_{abs} and g_{lum} values the exploitation of forbidden transitions, involving small electric-dipole transition moments, but large magnetic-dipole ones must be highlighted as useful, mainly in that concerning CPL emission [15]. However, such modulation can be significantly detrimental for the emission capability and, therefore, for B_{CPL} values. Hence, the participation of forbidden transitions needs to be finely adjusted for each specific design [18], in order to get a large enough B_{CPL} value.

BODIPYs are in the spotlight as useful small organic dyes. Despite featuring an inherently achiral (planar) chromophore, they have been intensively used to develop CP-active SOMs [19], mainly due to two fundamental factors. From a photophysical point of view, they possess strong light-absorption and -emission efficiencies, as measured by their large ε and φ values, respectively [20]. From a synthetic point of view, they have outstanding chemical versatility [21], which allows implementing visible chiroptical activity in the planar BODIPY chromophore by easily linking a number of chiral moieties to it [22–25], or by embedding it in helically-chiral architectures [26–28].

Related to the development of helically-chiral CP-active BODIPYs, we have established a simple approach, consisting of the easy mutual covalent linkage of two identical BODIPY chromophores through a short, flexible and chiral bridge based on ethane-1,2-diamine or −1,2-diol, to obtain ECD- and CPL-active C_2-symmetric helically-flexible bis (BODIPYs) (named *helico*BODIPYs; *e.g.*, **1a** and **2a** in Fig. 1) [29,30]. These *helico*BODIPYs are easily constructed by aromatic nucleophilic substitution of chlorine in accessible 3-chloroBODIPYs, using commercially enantiopure C_2-symmetric ethane-1,2-diamines or −1,2-diols, as the nucleophilic reagents [29]. Although *helico*BODIPYs involve two chiral centers in their structure (see Fig. 1), theoretical simulation pinpointed to the helical chirality as the main chiral factor behind their significant CP activity (noticeable visible ECD and CPL signals) [29,30]. Thus, in seminal *helico*BODIPY **1a**, with *S*,*S* configuration for their chiral centers, the involved BODIPY chromophores are disposed anti-clockwise in its preferred helical conformation (*M*), leading to a positive visible couplet (bisignalized ECD signal with a positive Cotton effect), which is in agreement with the prediction afforded by applying the ECD exciton chirality method [29,31]. Accordingly, the corresponding *R*,*R* enantiomer shows the opposite behavior, clockwise orientation of BODIPY chromophores in the preferred *P* molecular helix, which results in a negative ECD visible couplet.

Although the *helico*BODIPYs developed to-date exhibit a good capability to absorb light (ε values up to 10^5 $M^{-1}cm^{-1}$), they are characterized by a low fluorescence efficiency (φ up to 30 %, but decreasing in polar media) [29,30], probably due to the participation of CT emission induced by the push-pull character of the involved BODIPY chromophores (*e.g.*, note in Fig. 1 the presence of electron-donating nitrogen and electron-withdrawing chlorine atoms respectively localized at symmetrically-opposite α-pyrrolic BODIPY positions in **1a**). A fact supporting this hypothesis is the enhanced fluorescence efficiency of related **2a** [30], bearing less electron-donating oxygens instead of nitrogens (**1a** case) attached to the BODIPY chromophores (see Fig. 1). On the other hand, whereas the signs of the maximum g_{abs} and g_{lum} values are opposite for **1a** [29], they are equal for **2a** [30]. This fact and the

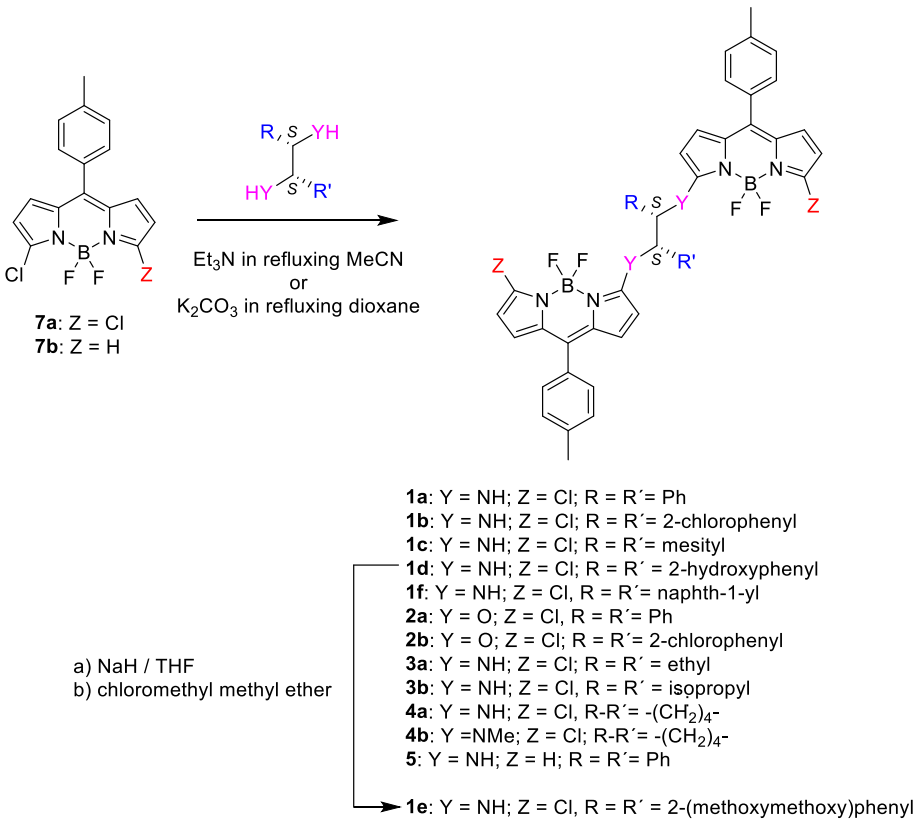

Scheme 1. Synthesis of *helico*BODIPYs. See ESI for experimental details.

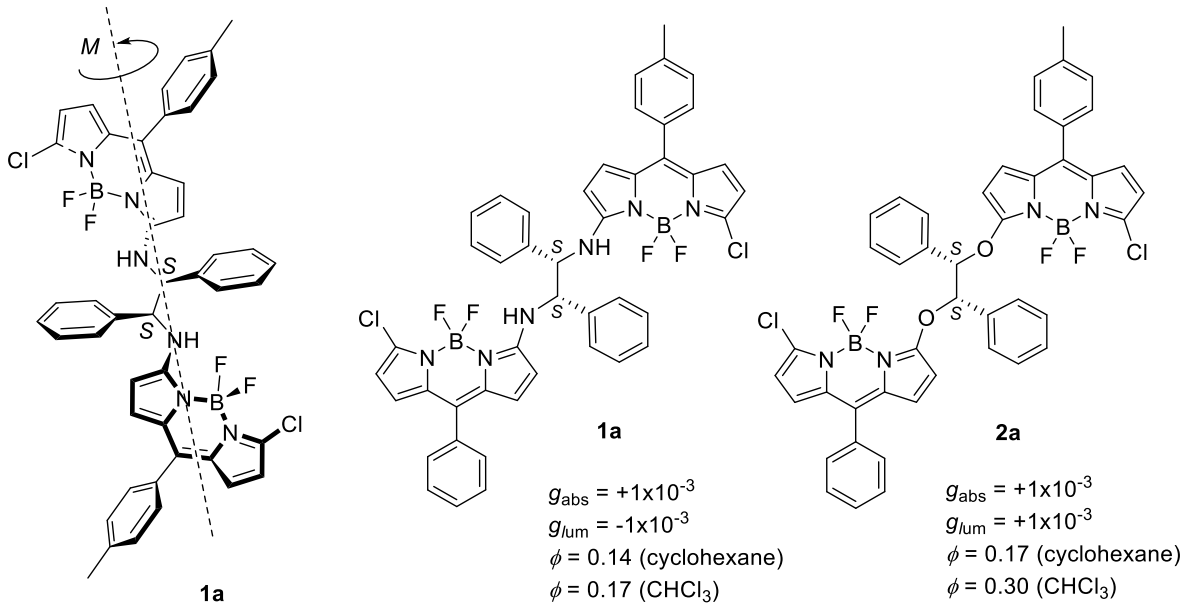

Fig. 1. Schematic view of the preferred *M* helical conformation (dotted line indicates the chiral axis) for *helico*BODIPY **1a** (*S*,*S*), as well as differential visible fluorescence efficiencies and maximum visible g_{abs} and g_{lum} values for **1a** and related **2a**.

differential dependence of the fluorescence efficiency of both dyes on the solvent polarity (see Fig. 1) pinpoint to enhanced participation of CT emission in the case of **1a**, as it also occurs in chiroptical BINOL-based monoBODIPYs with enhanced push-pull effects [32].

On the other hand, we have recently noticed that steric hindrance at the flexible bridge has a striking impact on the chiroptical signatures (ECD and CPL) of *helico*BODIPYs **1a-c** (Fig. 2) [33]. Thus, increasing the steric overcrowding at the bridge, by increasing the volume of the aryl moieties hanging from it, results in the elongation of the *helico*BODIPY molecular helix (helical pitch increase). This trend leads to a noticeable increase in the measured absolute g_{abs} and g_{lum} values, as well as it enables changes in their relative signs (*e.g.*, from maximum visible g_{abs} = 1.6 × 10^{-3} for **1a**, to 13.2 × 10^{-3} for **1c**, negative g_{lum} for **1a** *vs.* positive for **1b** or **1c**, in chloroform, see Fig. 2) [33].

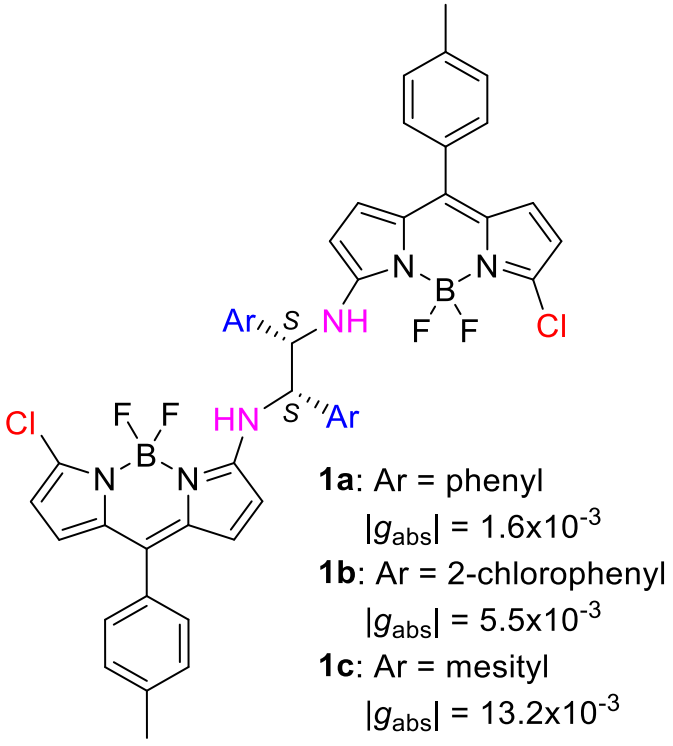

Fig. 2. Influence of the increase of the *helico*BODIPY helical pitch, by increasing the overcrowding at the flexible ethylene bridge, on the visible g_{abs} values (absolute values in chloroform) [32].

Moreover, seminal computations conducted by us on **1a** seemed to support participation of BODIPY-to-BODIPY CT in its main visible absorption band [29]. All this collected information prompted us to hypothesize that the underlying phenomenon behind the chiroptical changes observed upon the molecular helix elongation could be due to BODIPY-to-BODIPY CT. This CT could be promoted by an enhanced symmetry-breaking induced CT (SBCT) mechanism in *helico*BODIPYs having a proper disposition of their BODIPY units, as it also occurs in a number of BODIPY-BODIPY dimers [34]. Indeed, SBCT strongly depends on the distance and mutual orientation of the acting chromophores [35,36].

To investigate in depth the competitive or synergic participation of these three effects, helix elongation, BODIPY CT and BODIPY-to-BODIPY CT, on the valuable visible chiroptical activity of the readily-accessible *helico*BODIPYs, we have selected a battery of structurally related dyes (Fig. 3). This set includes previously reported *helico*BODIPYs (**1a-c** [29,33] and **2a** [30]), and unprecedented ones (**1d-f**, **2b**, **3a,b**, **4a,b** and **5**). All the molecular structures were chosen on the basis of synthetic accessibility factors. Thus, the at-bridge phenyl rotors of seminal **1a** have been replaced by *ortho*-substituted phenyls (**1b-e** in Fig. 3), benzo-fused phenyls (**1f**) and different alicyclic chains (**3a,b**) and cyclic (**4a,b**) alkyl chains to study the influence of the bridge overcrowding in the *helico*BODIPY conformation and, therefore, in the promotion of BODIPY-to-BODIPY CT. On the other hand, to study the possible influence of electronic factors in the BODIPY push-pull and, hence, in the BODIPY CT, different groups with dissimilar electronic effects have been linked to the BODIPY chromophores (cf. **1a**, **2a** and **5**). Additional structural changes leading to other stereoelectronic effects have been also included in the selected set of dyes, such as amino methylation (cf. **3a** and **3b**, or **4a** and **4b**), or the change of the highly-flexible 1,2-diphenylethene chiral bridge by less-flexible, related ones (cf. **1a** and **4a**).

This set of dyes should allow revealing the competitive participation of BODIPY CT *vs.* BODIPY-to-BODIPY CT, by experimentally and computationally studying the influence of the BODIPY push-pull, and

the BODIPY-BODIPY distance and disposition on the *helico*BODIPY photophysics and chiroptics (visible ECD).

2. Materials and methods

Detailed information about the used reagents, synthetic procedures and structural characterization of all the compounds, as well as on the spectroscopic techniques and computational calculations applied to record the photohysical and chiroptical signatures of the *helico*BODIPYs, is included in the electronic supporting information (ESI).

3. Results and discussion

3.1. Synthesis

Following the optimized procedure reported recently by us for the synthesis of **1b-c** [33], unprecedented enantiopure *helico*BODIPYs **1d-f**, **3a,b**, and **4a,b** were successfully synthesized by reacting 3,5-dichloro-8-(4-methylphenyl)BODIPY **7a** [37] with the corresponding commercial enantiopure (*S*,*S*)-diamine (1,2-bis(2-hydroxyphenyl)ethane-1,2-diamine for **1d**, 1,2-bis(napht-1-yl)ethane-1,2-diamine for **1f**, hexane-3,4-diamine for **3a**, 2,5-dimethylhexane-3,4-diamine for **3b**, cyclohexane-1,2-diamine for **4a**, and *N*,*N*′-dimethylcyclohexan-1,2-diamine for **4b**) in refluxing acetonitrile, in the presence of triethylamine as a base (see Scheme 1). The involved double aromatic nucleophilic substitution afforded the desired *helico*BODIPYs in chemical yields ranging from 48 % for **1f**, to 76 % for **4b**. Under the same reaction conditions, known **1a** [29] was obtained in an improved 64 % chemical yield from **7a** and commercial (*S*,*S*)-1,2-diphenylethane-1,2-diamine, whereas chlorine-free enantiopure **5** was obtained in a lower chemical yield (31 %) from 3-chloro-8-(4-methylphenyl)BODIPY **7b** [38] and the same diamine under the same conditions. The lower yield for **5** can be explained by the lower reactivity of monochlorinated **7b** when compared to dichlorinated (electron-poorer) **7a** towards nucleophilic substitution.

On the other hand, *helico*BODIPY **2b** was prepared from **7a** and commercial (*S*,*S*)-1,2-bis(2-chlorophenyl)ethane-1,2-diol in 45 % chemical yield, using the alternative conditions reported by us for the preparation of related **2a**, that is, refluxing 1,4-dioxane and K_2CO_3 instead of trimethylamine as the base [30]. These conditions avoid the

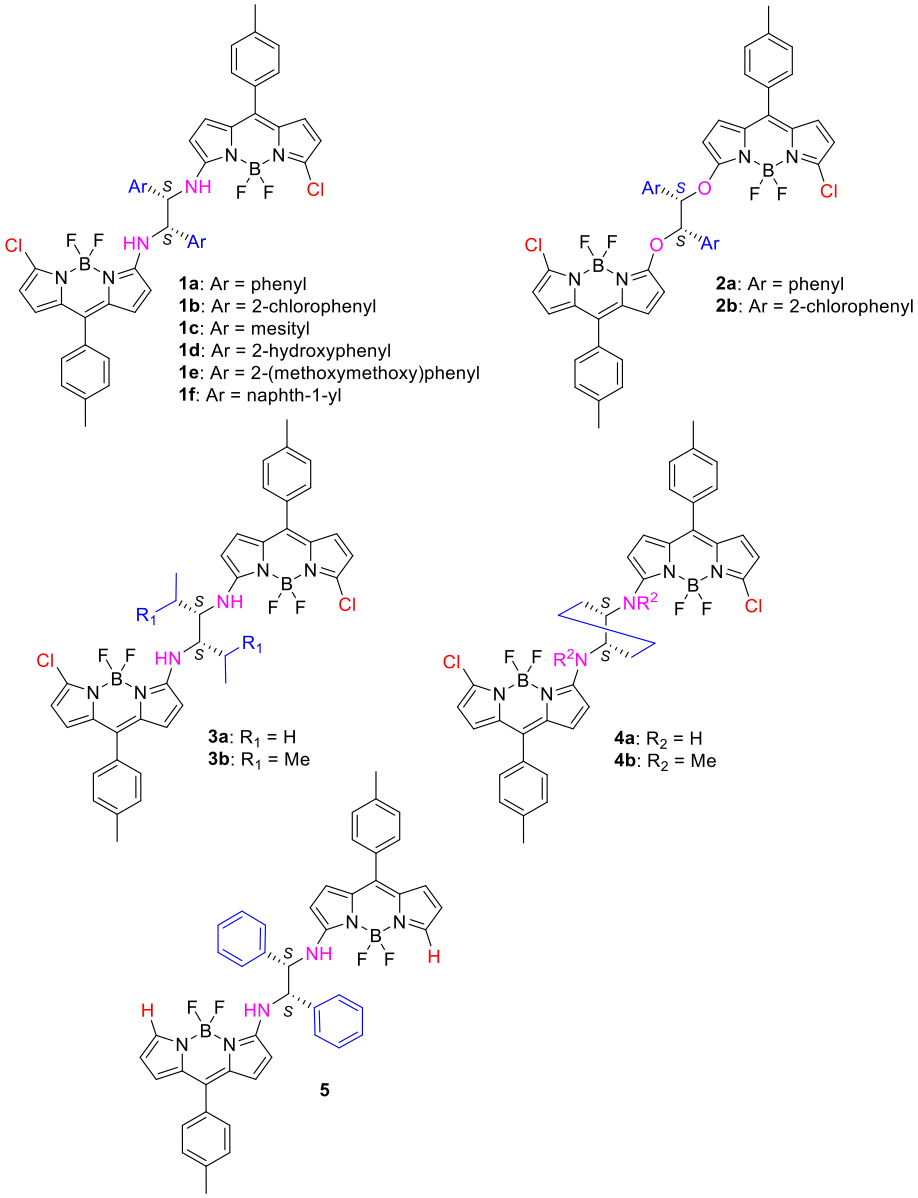

Fig. 3. Selected battery of *helico*BODIPYs.

competitive attack of triethylamine (yielding the corresponding 3-diethylaminoBODIPY) that takes place when less nucleophilic reagents, such as diols, are used. Finally, *helico*BODIPY **1e** was obtained from **1d** in 17 % chemical yield by a double standard Williamson etherification with chloromethyl methyl ether and sodium hydride.

3.2. Photophysical properties

All the selected new *helico*BODIPYs were photophysically characterized with the exception of 2-hydroxyphenyl-based **1d**, which was discarded to avoid artifacts due to the expected participation of different hydrogen-bonded species in solution, as supported by ^{1}H NMR analysis (note the possibility of intra- and inter-molecular hydrogen-bonding involving the hydroxyl groups).

In brief, the main photophysical signatures of seminal *helico*BODIPY **1a** (Fig. 1) are ruled by three key structural factors. On the one hand, amination of the BODIPY α-pyrrolic position modifies the vibrational resolution of the chromophore visible electronic transition, leading to broader and flattened spectral profiles [39–42], especially in polar media. On the other hand, the conformational freedom of the involved *meso*-*p*-tolyls (BODIPY *meso*-aryl rotors) favors non-radiative deactivation channels limiting the dye fluorescence response [20]. Finally, additional fluorescence quenching pathways are activated in polar media, where the fluorescence response tends to zero owing to solvent-induced stabilization of CT processes [36].

Firstly, to ascertain the main operative CT mechanism in *helico*BODIPYs (push-pull-enabled BODIPY CT *vs*. SBCT-enabled BODIPY-to-BODIPY CT), we selected dyes with expectedly different push-pull strengths. In particular, we compared **1a** with **5** and **2a,b**, where 1a (with electron-donating nitrogen and electron-withdrawing chlorine) is expected to have a stronger push-pull than **5** (without chlorine) or **2a,b** (with less electron-donating oxygens) (see Fig. 3). Indeed, the replacement of the bridge nitrogens by oxygens slightly ameliorated the fluorescence response, mainly in apolar media (*e.g.*, cf. **2a** *vs.* **1a**, in Table 1), as it was expected due the lower push-pull character of the oxygenated BODIPYs chromophores in **2a,b**. However, the removal of the electron-withdrawing chlorines in **5** did not induce the expected improvement in its fluorescence response, which was even worse than the recorded for **1a** (Table 1). Moreover, the fluorescence efficiency of **2a,b** and **5** was still very sensitive to the solvent polarity, yielding very low fluorescence quantum yields in polar media, as a result of the fluorescence quenching induced by the solvent stabilization of the feasible CT state (see Tables S1 and S2 in ESI). It has been reported that amino groups alone are able to induce CT processes in BODIPY chromophores, but when bonded to the chromophoric β-pyrrolic BODIPY position [43]. Therefore, in spite of the strong push-pull character of the BODIPY units of **1a**, the observed CT must occur between the two BODIPY units by a preferred SBCT mechanism, but not within a single one. Noteworthy, as above mentioned, SBCT has been claimed as the main solvent-driven non-radiative de-excitation channel in covalently linked BODIPY-BODIPY dyads [34–36].

Table 1
Photophysical signatures (absorption, λ_{ab}, and fluorescence, λ_{fl}, wavelengths; molar absorption, ε_{max}; fluorescence quantum yield, φ; and fluorescence lifetime, τ) of the *helico*BODIPYs depicted in Fig. 3 in diluted solution of cyclohexane. Data in other solvents are collected in Tables S1–S3 in ESI.

	λ_{ab} (nm)	$\varepsilon_{max}\cdot10^{-4}$ ($M^{-1}cm^{-1}$)	λ_{fl} (nm)	φ	τ (ns)
1a [29]	529.0	12.4	544.0	0.17	1.15 (97 %) – 4.70 (3 %)
1b [32]	525.0 483.0	5.7 5.4	540.5	0.28	1.00 (86 %) – 2.55 (14 %)
1c [32]	533.0 484.5	5.3 7.1	547.0	0.25	0.71 (70 %) – 2.98 (30 %)
1e	524.5 470.0	9.5 8.0	552.0 578.0	0.40	1.35 (75 %) – 5.95 (25 %)
1f	530.5 487.0	6.0 6.2	544.0	0.29	0.98 (86 %) – 3.40 (14 %)
2a [30]	516.0	12.2	523.5	0.30	0.75 (63 %) – 1.75 (37 %)
2b	516.0	10.1	525.5	0.25	1.93
3a	532.0	7.3	549.5	0.26	1.68 (97 %) – 5.63 (3 %)
3b	528.0 475.0	7.4 4.7	544.5 582.5	0.31	1.33 (86 %) – 5.56 (14 %)
4a	530.0 473.5	7.7 4.4	552.5 580.5	0.35	1.36 (56 %) – 4.09 (44 %)
4b	535.0	9.3	568.0	0.03	0.11
5	522.5 490.0	9.2 4.2	539.5	0.10	0.50

3.2.1. HelicoBODIPYs involving an arylated bridge

First, regarding the *helico*BODIPYs with nitrogenated bridges (**1**), it is found that the conformational restriction of the phenyls at the bridges, induced by the phenyls *ortho*-substitution with bulky groups (chlorine in **1b**, methyl in **1c**, or methoxymethoxyl in **1e**) or by their benzo-fusion (**1f**), has a marked impact in the profile of the *helico*BODIPY visible absorption band, as shown in Fig. 4.

In order to understand this differential behavior, the ground-state optimized geometries of all of the new *helico*BODIPYs bearing sterically constrained nitrogenated bridges (**1b,c** and **1e,f**), as well as the molecular orbitals involved in the absorption transition, were computed (PCM/CAM-B3LYP-6-311G*; see ESI for details). The modelizations show helical conformation for all dyes, analogous to that previously demonstrated for **1a** [29]. However, the distance between BODIPY chromophores in the new dyes is longer than it was in **1a** (distance between the centers of masses of *ca.* 10 Å; see Fig. 5, and Fig. S2 in ESI), being the BODIPY units no longer coplanar (BODIPY-BODIPY dihedral angle ranging from *ca.* 60° to *ca.* 75°; see Fig. 5 and Fig. S2 in ESI).

Moreover, in addition to the expected main absorption band (around 520–530 nm), resulting from the additive HOMO-1 → LUMO and HOMO → LUMO+1 transitions (TD PCM/CAM-B3LYP-6-311G*; see ESI for details), both within a single BODIPY unit (see Fig. 5, and Fig. S3 in ESI), a new one is recorded at shorter wavelengths (460–480 nm; see Fig. 4, and Fig. S1 in ESI). This new short-wavelength band is especially prominent for **1c**, featuring the most constrained bridge (involving highly bulky pendant mesityls; see Fig. 3), being ever higher than the said, and common long-wavelength BODIPY absorption. Note that this new hypsochromic band is not so prominent in the corresponding monoBODIPYs carrying the bridge, which exhibit absorption profiles that are flattened and broadened by the electron coupling exerted by the bridge's amino group linked to the C3 BODIPY position (as representative examples, see the spectra of helicoBODIPYs **1b** and **1c**, and their corresponding monoBODIPYs **m-1b** and **m-1c**, in Fig. S4 in ESI). Therefore, the growing of such short-wavelength absorption for the *helico*BODIPYs involving sterically-hindered bridges should be related to a BODIPY-BODIPY intramolecular interaction within the covalently-linked BODIPY subunits.

An increase of the solvent polarity favors the new short-wavelength band in detriment of the common long-wavelength one (see Fig. 4). Such a drastic change in the shape of the absorption spectrum cannot be assigned solely to the amino-induced changes in the vibrational resolution of the BODIPY visible absorption band, resulting from its electronic coupling through the BODIPY 3 position [39–41], but it pinpoints to the participation of an additional chromophoric entity with its own absorption profile. Indeed, the replacement of the strongly electron-donating nitrogens of **1b** (*helico*BODIPY with bulky 2-chlorophenyls at the bridge) by less electron-donating oxygens in **2b** does not enhance the short-wavelength band upon polarity increase (see Fig. S5 in ESI). Even more, the visible absorption pattern of **2b** resembles those of **1a** or **2a**, the latter bearing less overcrowded bridges (see Figs. S1A and S5 in ESI). All these findings suggest that the bridge-induced geometrical disposition of the BODIPY subunits in the *helico*BODIPY architecture plays a key role in the dye light-absorption signatures.

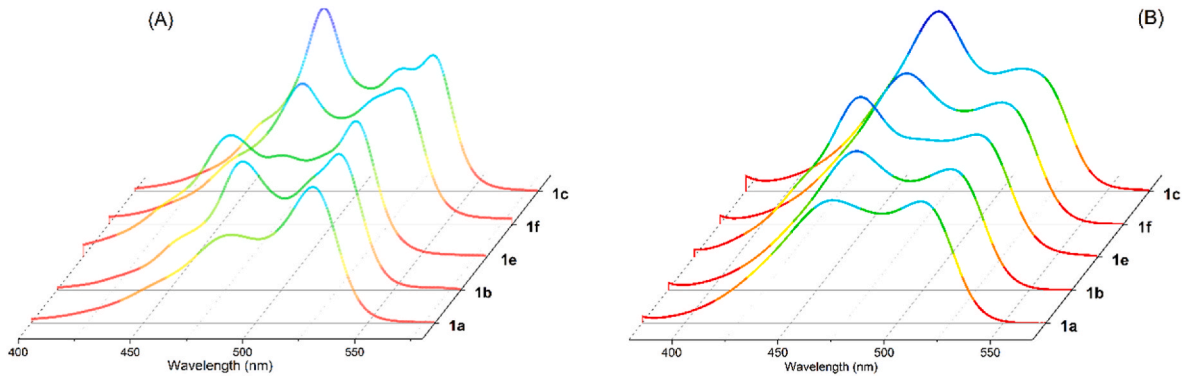

Fig. 4. Normalized (by the long-wavelength band intensity) visible absorption spectra of *helico*BODIPYs **1b-c** and **1e-f**, bearing bridges with bulky aryls, in non-polar cyclohexane (A) and in polar methanol (B). The corresponding spectra of **1a**, with unconstrained non-substituted phenyls, are included for comparison purposes. Absorption spectra in other solvents are shown in Fig. S1 in ESI.

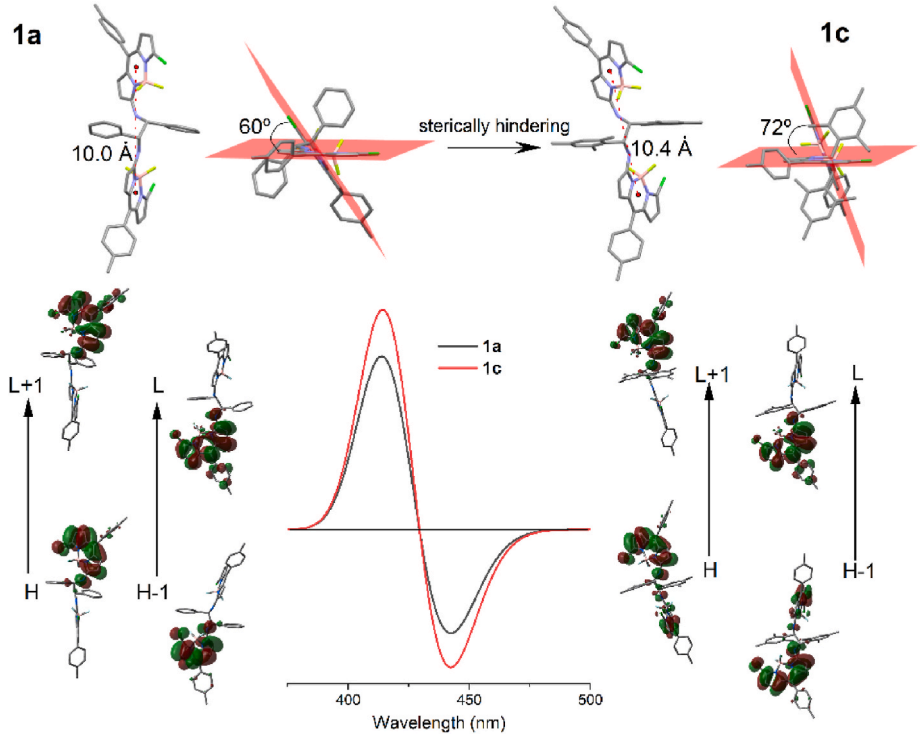

Fig. 5. Computed (PCM/CAM-B3LYP/6-311G*) ground-state geometries and electron-density contour maps of key molecular orbitals (H: HOMO and L: LUMO), as well as theoretically-predicted ECD spectra in chloroform (TD PCM/CAM-B3LYP/6-311G*) of representative **1a** and **1c** (*R*,*R* enantiomers were computed). Key computed geometrical parameters (distance between the center of masses of the BODIPY chromophores, and dihedral angle between the BODIPY chromophore planes) are included. Optimized geometries and orbital contour maps for the rest of the selected *helico*BODIPYs with arylated bridges are depicted in Figs. S2 and S3 in ESI, respectively.

Regarding emission, the visible fluorescence spectra of this set of *helico*BODIPYs (based on arylated bridge, see Fig. 3) remind of that recorded for seminal **1a** (see Fig. S1 in ESI), with the exception of **1e** bearing methoxymethoxyl as pendant chain in its bridge phenyls. Thus, a new bathochromically-shifted visible band (at *ca.* 570–580 nm) was detected for **1e** in non-polar media, together with the common *helico*BODIPY emission centered at 540–550 nm (Fig. 6A). Considering, that CT-states are further stabilized at the excited state, the new, long-wavelength emission of **1e** must be attributed to CT fluorescence. Nonetheless, in all these cases increasing the solvent polarity implies a significant reduction of the emission intensity, owing to the fluorescence quenching afforded by the working CT, but the spectral profiles still resemble that of parent **1a** (see Fig. S1 in ESI).

To better support that the recorded visible new absorption and fluorescence bands are owned to the same excited state, we recorded the fluorescence and excitation spectra of **1e** at different excitation and emission wavelengths in apolar cyclohexane (see Fig. 6). We selected this *helico*BODIPY because it shows the clearest dual fluorescence emission (*i.e.*, common short-wavelength band together with the non-common long-wavelength one). In the fluorescence spectra (Fig. 6A), as the excitation wavelength becomes lower (down to 480 nm), and hence approaching the region of the new absorption band (at 470 nm), the long-wavelength emission (at *ca.* 580 nm) increases with respect to the short-wavelength one (at 550 nm). Accordingly, in the excitation spectra (Fig. 6B), as the monitoring emission wavelength becomes higher (up to 630 nm), hence the region where the new emission band is dominating, the non-common short-wavelength absorption band (at 470 nm) increases in the excitation spectra.

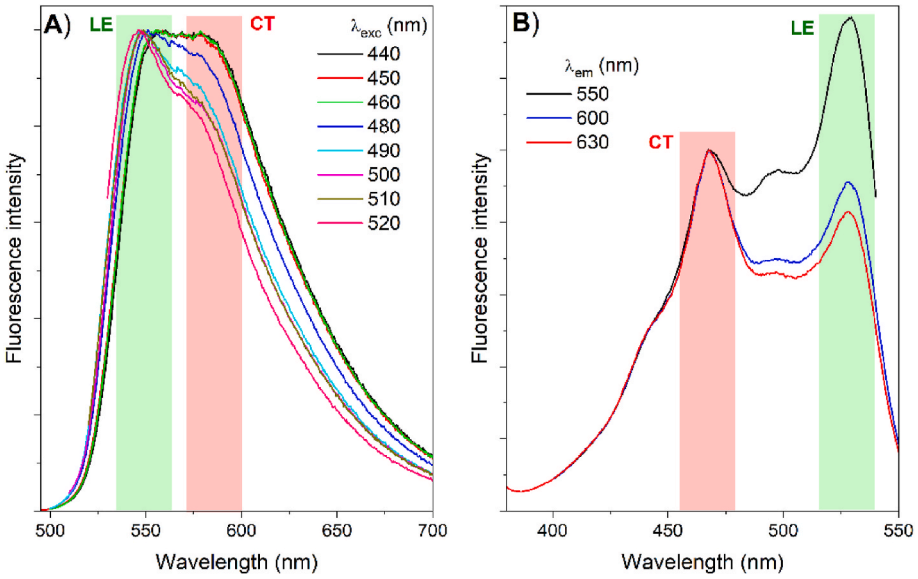

Fig. 6. Fluorescence (A) and excitation (B) spectra of **1e** in cyclohexane at different excitation and emission wavelengths, respectively.

All these results support the participation of the same excited state in both new absorption and emission bands, as well as the participation of a single chromophoric entity, the BODIPY-BODIPY dyad enabling CT by the SBCT mechanism. Thus, depending on the steric hindrance at the bridge, the dynamics and population availability of the SBCT state change, and even its direct population from the ground state (short-wavelength absorption band in Fig. 4), and its emissive de-excitation (long-wavelength emission in Fig. 6A for **1e**) can be detected in some cases under specific conditions. This new hypsochromic absorption band is also recorded in viscous media such as ethylene glycol (for example see Fig. S6 in ESI, for representative *helico*BODIPYs **1b** and **1c**), being the spectra registered in ethylene glycol similar to those in methanol (Fig. 4). Indeed, the fluorescence signals in this viscous and polar solvent are as low as in methanol (efficiency <1 %) and located in the same spectral region (Fig. S6 in ESI). Therefore, the origin of such absorption should be related to media polarity rather than to viscosity, discarding the involvement of different conformers in solution, and once again sustaining SBCT as the origin of the new transition and fluorescence quenching channel. In this context, proper and fixed BODIPY-BODIPY orientations, adopted in constrained conformations involving over-crowded bridges, seems to be key in the dynamics and feasibility of the BODIPY-BODIPY SBCT. In fact, the theoretically optimized geometries of the studied *helico*BODIPYs suggest that the higher the sterical hindrance at the bridge, the more orthogonal the disposition of the BODIPY chromophores (*e.g.*, BODIPY-BODIPY dihedral angle ranging from 60° in less-hindered phenyl-based **1a**, to 72° in more-hindered mesityl-based **1c**; see Fig. 5). It must be remarked here that the SBCT mechanism is especially favored in orthogonal BODIPY-BODIPY dyads [36]. To further support SBCT occurrence, we have measured the electrochemical properties of a series of representative *helico*BODIPYs and corresponding related monoBODIPYs carrying the bridge moiety by cyclic voltammetry. The registered oxidation and reduction *helico*BODIPY potentials are almost identical to those registered for the corresponding monoBODIPYs carrying the same bridge, as well as to those previously reported for other monoBODIPYs [44], and significant new potential waves were not detected, especially in the case of the *helico*BODIPYs (as a representative example, see the voltammograms of *helico*BODIPY **1b** and its corresponding monoBODIPY **m-1b** in Fig. S7 in ESI). This electrochemical behavior suggests that the ongoing CT does not require a strongly-coupled and electronically well-defined pair of electron donor and electron acceptor, but it rather takes place between a weakly-coupled pair of identical chromophores by a process which is not driven by electrostatic forces, such as the SBCT one.

It must be also noted that the SBCT mechanism implies a significant stabilization of the CT excited state by a strong charge separation within it, driven by environmental and structural factors. This high CT stabilization allows the detection of the above mentioned long-wavelength CT emission in the case of **1e** (Fig. 6). Further CT state stabilization by increasing the solvent polarity favors both its population and the charges separation within it, but also decreases the CT emission, since the larger the charge separation, the lower the probability of charge recombination that is required for CT emission [45,46]. For the rest of these *helico*BODIPYs, the corresponding CT state does not emit in any of the tested solvents, or the long-wavelength CT emission is too weak and masked under the LE fluorescence (see Figs. S1 and S8 in ESI). Thus, in these last cases, the corresponding excitation and fluorescence spectra are independent of the excitation and emission wavelengths, respectively (for example, see the spectra of **1b** in Fig. S5 in ESI).

Therefore, the recorded new visible absorption band would originate from the direct population of a CT state in the BODIPY-BODIPY chromophoric system by the SBCT mechanism. The theoretical simulation (TD DFT) is not able to sustain such band splitting, and just a single main visible absorption is predicted. However, the frontier molecular orbitals (FMOs) involved in such absorption, and the contributions of the corresponding transitions, depend on the sterical hindrance at the bridge. As aforementioned, the recorded absorption is the result of the additive contributions of the HOMO-1 → LUMO and HOMO → LUMO+1 transitions, whose molecular orbitals are located in a single BODIPY subunit. However, in the *helico*BODIPYs with the most sterically-hindered bridges (**1b** or **1c**) an additional contribution of the HOMO → LUMO transition is predicted (*ca.* 15 % contribution). The latter transition implies a marked shift of electronic density from one BODIPY unit to the other (see Fig. 5 and Fig. S3 in ESI). Besides, in these *helico*BODIPYs the HOMO and HOMO-1 are slightly extended throughout both BODIPY units (albeit the electronic density is preferably and alternatively located in one of them), whereas the LUMO and LUMO+1 are exclusively and alternatively placed in a single BODIPY unit (see Fig. 5 and Fig. S3 in ESI). Therefore, even the main visible transitions of these *helico*BODIPYs involve some shift of electronic density, from a BODIPY unit to the other one, proving CT character to the absorption. This CT state would be energetically located over the locally-excited (LE) state (Fig. 7), as supported by the spectral position of these new absorption bands (Fig. 4). However, upon excitation, the relative position of such a CT and LE states would reverse, the CT becoming the low-lying one (Fig. 7) and

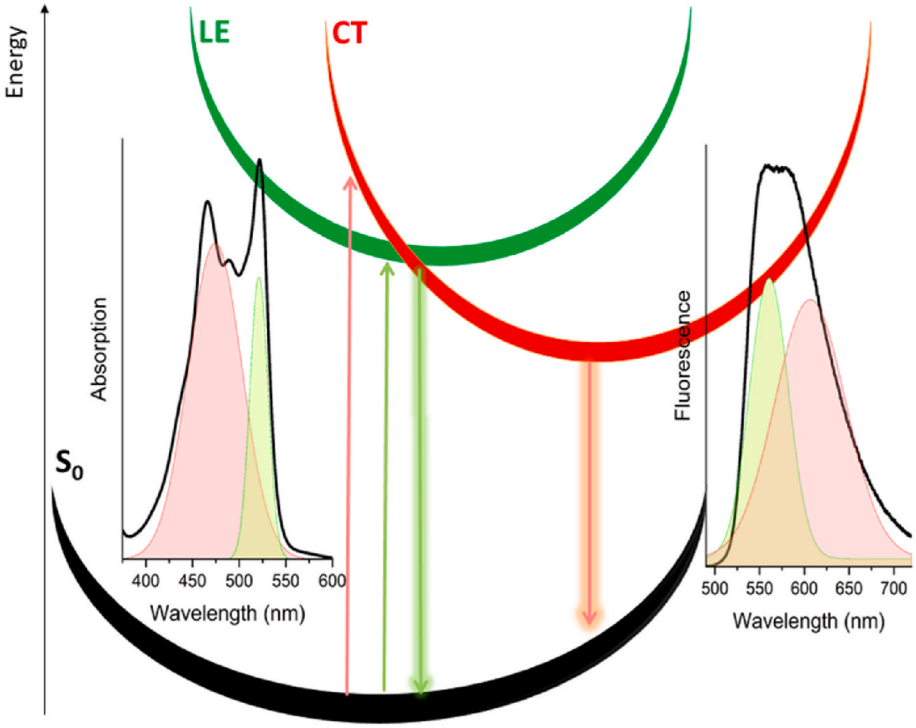

Fig. 7. Cartoon explaining the origin (CT promoted by SBCT) and spectral position of the additional visible absorption and emission bands recorded from *helico*BODIPYs. Upon direct population of the enabled CT, this state relaxes below the LE. The visible absorption and fluorescence spectra of **1e** in cyclohexane (as archetype of SBCT-enabling *helico*BODIPY), deconvoluted in two Gaussians, are included to show the contribution and spectral position of each electronic transition.

leading to bathochromically shifted CT emissions, as supported by the found spectral disposition of the new visible emission bands for **1e** (see Fig. 6A). It must be noted here that, in a number of molecular systems, even those involving BODIPY chromophores, the direct population of CT states from the S_0 ground state was recorded in the corresponding absorption spectra as a hypsochromic shoulder overlapping with the band corresponding to the direct population of the LE state [43,47].

It is noteworthy that the key participation of a CT state in the visible absorption and fluorescence of the *helico*BODIPYs not only depends on the environmental polarity, but also on the bridge-controlled *helico*BODIPY helical conformation (proper disposition of the involved BODIPY units to promote SBCT). As a matter of fact, CT absorption is better visualized when bulky mesityls are involved in the *helico*BODIPY bridge (see **1c** in Fig. 4), whereas CT fluorescence is better monitored when less bulky 2-(methoxymethoxy)phenyls are in the bridge instead of mesityls (see **1e** in Fig. 6A). In other words, a critical balance of steric and polar effects must be achieved to enhance BODIPY-to-BODIPY SBCT in *helico*BODIPYs, and to allow the recording of the corresponding CT-state involved spectral bands.

With regard to fluorescence efficiency and excited-state dynamics, all these *helico*BODIPYs follow the expected trends (*e.g.*, see Table 1 for **1a-c, 1e,f** and **2a,b**). Thus, they display a moderately-bright visible fluorescence in non-polar media (φ around 15–30 %), with main lifetimes (τ) of *ca.* 1 ns (as found from the biexponential fit of the fluorescence decay curve), owing to the fluorescence quenching afforded by the free motion of the BODIPY *meso*-*p*-tolyl rotors outlined previously [20]. Increasing the solvent polarity results in almost negligible emissions with fast lifetimes (beyond the time-resolution of the disposable photon counter), due to effective fluorescence quenching induced by the polarity-driven increased stabilization and participation of the CT state (see Table S1 and Table S2 in ESI). However, some remarkable differences are observed depending on the bridge steric overcrowding. Thus, increasing the steric hindrance exerted by the bridge pendant moieties results in a slight enhancement of the fluorescence quantum yields in non-polar media (from 17 % for **1a**, to *ca.* 30 % for **1e**; see Table 1). This could be easily explained by a more restricted conformational mobility for **1e**, due to the involvement of a more constrained bridge, which would reduce the participation of non-radiative de-excitation pathways associated to internal conversion. However, CT population must be the main fluorescence quenching mechanism in *helico*BODIPYs having overcrowded bridges, where the SBCT mechanism is significantly promoted, as it is shown experimentally (Table S1 in ESI). Thus, even in solvents of medium polarity (*e.g.*, chloroform), the fluorescence quantum yield of these overcrowded *helico*BODIPYs is lower than 5 %, whereas in parent **1a**, with unhindered bridge phenyls, it was around 15 % (*e.g.*, cf. **1a** *vs.* **1b,c** and **1f** in Table S1 in ESI). An exception to this trend is the polarity-dependent behavior of overcrowded **1e** (see Table S1 in ESI). However, it must be noted that, in this case, significant CT emission is recorded together with the LE fluorescence, making the recorded fluorescence quantum yield of **1e** non-comparable, and probably overestimated due to the joint recording of the dual (CT and LE) emission. Further increase of the solvent polarity almost entirely suppresses the fluorescence response ($\varphi < 0.5$ %; Table S1 in ESI), a common trend in *helico*BODIPYs owing to the quenching by the "dark" CT in polar enough environments, where the charges separation is roughly favored.

3.2.2. *HelicoBODIPYs involving an alkylated bridge*

In view of the fundamental role played by the bridge pendant groups (steric effect), the phenyls in ethane-1,2-diamine-based bridges were replaced by alkyl chains (linear in **3a**, branched in **3b** and cyclic in **4a** and **4b**; the latter involving methylated nitrogens). The spectral profiles and photophysical signatures of **3a**, the *helico*BODIPY with the less-hindered alkylated bridge, resemble those recorded for parent **1a** (see Fig. 8 and Table 1). However, in *helico*BODIPYs **3b** and **4a**, bearing bulkier alkyls, marked changes are detected in both the visible absorption and fluorescence spectra, mainly in polar media (see Fig. 8): On the one hand, a growing absorbance at short wavelengths (once again around 460–475 nm) in non-polar solvents. On the other hand, a dual fluorescence emission, also in non-polar solvents, due to the appearance

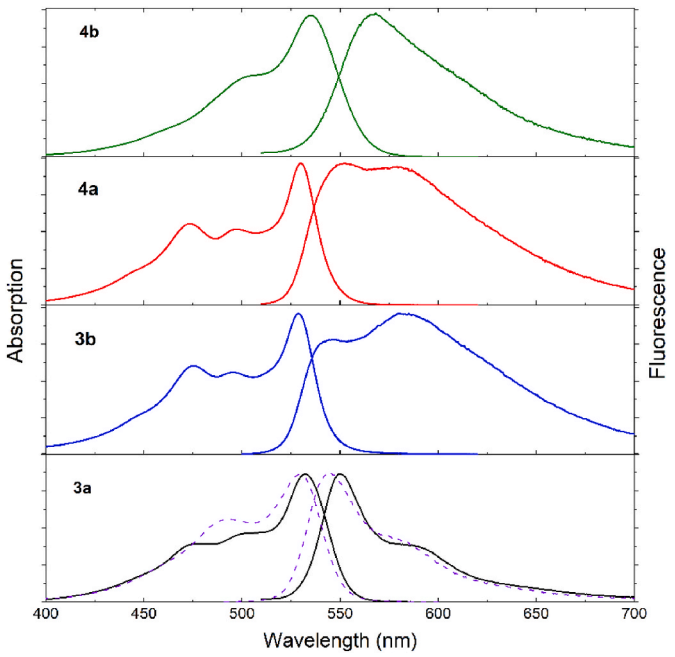

Fig. 8. Normalized absorption and fluorescence visible spectra of *helico*BODIPYs **3a,b** and **4a,b**, bearing alkyl chains hanging from their flexible bridges, in cyclohexane. The corresponding spectra of parent *helico*BODIPY **1a** are also included for comparison (purple, dashed). The corresponding spectra in other solvents are shown in Fig. S9 in ESI.

of a new, long-wavelength emission at *ca.* 580 nm (*i.e.*, batochromically flanking the LE emission at 540–550 nm).

These spectral trends for the bridge-overcrowded alkylated *helico*BODIPYs fully remind those observed for bridge-overcrowded arylated **1e** (cf. Figs. 4 and 6). Therefore, once again, increasing the bridge overcrowding seems to promote SBCT, enabling direct CT population by light absorption from the ground state and CT emission, and allowing the detection of CT-absorption and CT-emission bands in solvents of low polarity. Moreover, once again, further increasing the solvent polarity enhances the stabilization and charges separation of the CT state, converting it to a dark (non-emissive) CT state, and hampering the detection of CT fluorescence. Following the aforementioned trends, promotion of CT participation by SBCT entirely quenches the emission of overcrowded alkylated *helico*BODIPYs **3b** and **4a** in polar media (Table S3 in ESI). It must be remarked here that, once again, the fluorescence response of these SBCT-enabling *helico*BODIPYs shows a higher sensitivity to the media polarity when compared to less-overcrowded related **3a**, and their fluorescence quantum yields become very low even in solvents of medium polarity (*ca.* 3 % in chloroform; see Table S3 in ESI). Nonetheless, CT absorption is still detected, and even prevails in the absorption spectra of **3b** and **4a** in polar media (see Fig. S9 in ESI).

Finally, *N*-methylation in **4b** should lead to a more constrained bridge when compared to **4a** (see Fig. 3). However, no splitting of the absorption bands, owing to CT absorption, is detected for **4b** in apolar ciclohexane, and its visible absorption profile is sharp and matches that of parent **1a** (see Fig. 8, and Fig. S9 in ESI). Indeed, the molar absorption of **4b** approaches the value found for **1a** in this solvent, being the highest absorption among the *helico*BODIPY set bearing alkylated bridges (see Table 1). Moreover, the visible fluorescence spectrum of **4b** features a single band, which is slightly red-shifted with regard to the LE emission of related **3a,b** and **4a** (*e.g.*, see Fig. 8). Even more, the fluorescence efficiency of **4b** is very poor, even in non-polar media ($\varphi < 2.5$ %; see Table 1, and Table S3 in ESI). Such behavior is intriguing and, apparently, **4b** does not follow the trends observed for the rest of the studied *helico*BODIPYs, where the involvement of overcrowded bridges induces prominent changes in the spectral profiles (especially in absorption). Thus, it seems that the conformation of **4b** does not allow direct CT population from the ground state. In contrast, CT population appears to be highly favored upon excitation, giving place to a highly stabilized CT state (*i.e.*, with a significant charge separation), which assures a drastic quenching of the fluorescence emission (note that the CT state becomes an almost dark excited state, and its emission is so weak that it cannot be recorded). In fact, the computed preferred conformations of the *helico*BODIPYs bearing cyclohexane-based bridges (**4a,b**) differ from those computed for the *helico*BODIPYs bearing acyclic dialkylethane-based bridges (**3a,b**) (Figs. S10 and S11 in ESI). Thus, whereas **3a,b** preferably adopt the extended helical conformation previously observed for *helico*BODIPYs bearing arylated spacers (**1** and **2**), the cyclization of the bridge in **4a,b** induces a pleated conformation with the BODIPY units getting closer to each other (intramolecular distance between center of masses falls down to 5–6 Å). Moreover, the electronic density in FMOs is spread over both BODIPY units, suggesting the viability of intramolecular excitonic interactions, whereas for the unoccupied FMOs the electronic density is localized preferably in just one BODIPY (Fig. S11 in ESI). Therefore, we cannot exclude the formation of intramolecular J aggregates in **4a** and **4b**, where the cyclic bridge brings both BODIPY close enough and with the required geometrical arrangement (Fig. S10 in ESI) to undergo a head-to-tail intramolecular excitonic interaction, as it is pointed out by the spread occupied FMOs along both chromophores (Fig. S11 in ESI). Usually, the excitonic coupling in J aggregates usually leads to allowed long-wavelength absorptions, which have not been observed in any of the registered absorption spectra (Fig. 8 and Fig. S9 in ESI). However, J aggregation can be induced upon excitation, and stabilized by the BODIPY-BODIPY CT. In this context, the formation of emissive J aggregates could explain the unexpected red-shifted narrow fluorescence band recorded for **4b** in non-polar media (Fig. 8). Further increasing the media polarity stabilizes the SBCT and the J aggregate becomes non-fluorescent. All these photophysical and computational findings reinforce the dramatic role of the flexible bridge as controller of the *helico*BODIPY helical conformation (BODIPY-BODIPY disposition), and its impact in CT population and dye photophysics.

3.3. Visible electronic circular dichroism

Regarding visible ECD, all the new h*elico*BODIPYs involving arylated ethane-1,2-diamine-based bridges (**1e,f** and **5**; see structures in Fig. 3) follow the trends previously recorded for **1a-c** [29,33]. Thus, all of the synthesized *S,S* enantiomers display a clear visible positive couplet, with maximum molar ellipticities (θ) ranging from *ca.* 2.9×10^4deg cm^2 dmol^{-1} for **1e**, up to *ca.* 182.0×10^4 deg cm^2 dmol^{-1} for **1c** in diluted chloroform solution (Fig. 9A). The same trend is found for the *helico*BODIPYs **3a,b** bearing alkylated ethane-1,2-diamine-based bridges (see structures in Fig. 3, and the corresponding ECD spectra in Fig. S12 in ESI). As mentioned in the introduction, these visible couplets are due to an efficient chiral exciton coupling between the involved BODIPY chromophores, which are closely disposed in the corresponding, *M*-preferred helical conformation. However, in the case of *helico*BODIPYs **4a,b**, bearing cyclohexane-1,2-diamine-based bridges, different behavior was observed. Thus, whereas *S,S-helico*BODIPY **4a** follows the expected trend and exhibits the common positive couplet, *S,S–N,N′*-dimethylated **4b** (cf. **4a** and **4b** in Fig. 3) shows a sign reversal for the couplet (see Fig. 9B).

Strikingly, the visible ECD spectra of all the *S,S-helico*BODIPYs bearing nitrogenated BODIPYs (**1**, **3**, **4** and *5*) exhibit an small positive band (negative in the case of ECD-reversal **4b**) located at around 500 nm, between the two branches of the recorded visible couplet (see Fig. 9). The same band is detected in the *S,S-helico*BODIPYs bearing oxygenated BODIPYs (**2**; cf. Figs. 9 and 10), but with higher relative intensity in the latter. This band is ascribed to the above-mentioned short-wavelength CT absorption, which is better detected in the ECD spectra than in the absorption spectra due to its more forbidden character when compared to the LE absorption. It must be taken into account

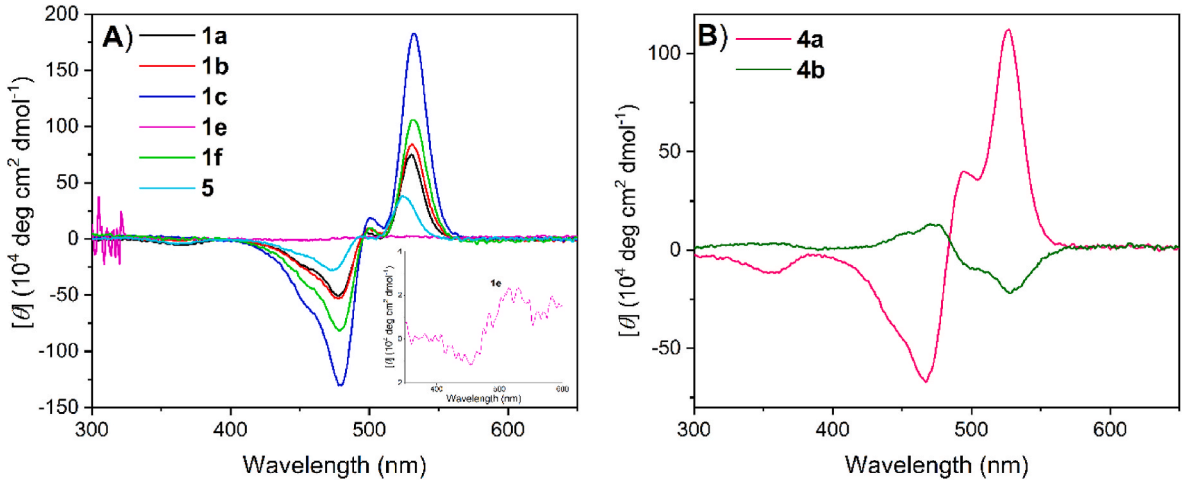

Fig. 9. Visible ECD spectra of ethane-1,2-diamine-based *helico*BODIPYs **1a-c, 1e,f** and **5** (A) and cyclohexane-1,2-diamine-based **4a,b** (B), all them with *S,S* configuration and bearing arylated bridges, in chloroform. Inset: zoom of the ECD spectrum of **1e**. See ESI for experimental details.

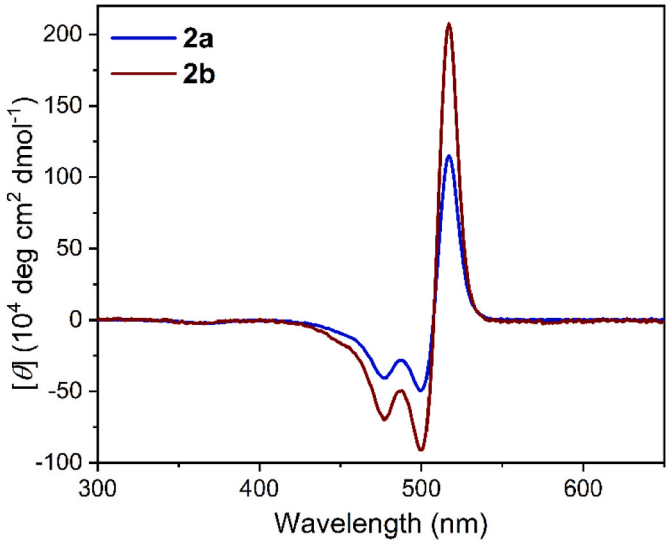

Fig. 10. Visible ECD spectra of ethane-1,2-diol-based *helico*BODIPYs **2a,b**, both with *S,S* configuration and bearing arylated bridges, in chloroform. See ESI for experimental details.

that the differential detection of this band (a single branch of the expected CT absorption couplet) within the LE couplet does not only depend on the differential probability of CT (higher for the dyes based on nitrogenated BODIPY), but also on the differential relative position of the CT couplet within the LE one. Thus, only one of the branches of the CT couplet is clearly recorded in all cases, its intensity depending on its probability and differential interference with the LE couplet, whereas the other branch (positive or negative) is totally masked under one of the LE couplet branches.

To better assess the influence of the bridge overcrowding on the visible ECD signatures, avoiding artifacts due to differential molar absorption, the corresponding maximum g_{abs} values ($g_{abs}(\lambda) = 2(\varepsilon_L - \varepsilon_R)/(\varepsilon_L + \varepsilon_R)$, where ε_L and ε_R are the molar absorptivity of left- and right-handed circularly polarized light) were compared instead of maximum θ values (Table 2). As it has been recently shown for *helico*BODIPYs **1a-c** [33], the at-bridge arylated *helico*BODIPYs, **1a-c** and new **1e,f** exhibit the expected trend: the stronger the bridge overcrowding (increased steric volume and restricted mobility of the bridge pendant moieties), the higher the maximum g_{abs} value (see Table 2). Thus, the found absolute g_{abs} values range from *ca.* 0.2×10^{-3} for **1e** up to 13.2×10^{-3} for **1c**, with the most overcrowded phenyls at the bridge (see Table 2). This $|g_{abs}|$ trend can be now better understood by the demonstrated enhanced CT absorption as the bridge overcrowding increases, and considering that the electronically forbidden character of such a transition should induce a higher dichroism.

Table 2
Maximum visible g_{abs} values for the selected *helico*BODIPYs (see structures in Fig. 3) in diluted chloroform solution (spectral position dated within parentheses).

	$g_{abs} \times 10^3$ (λ in nm)
1a	+1.6 (530)[a]
1b	+5.5 (531)[a]
1c	+13.2 (532)[a]
1e	+0.2 (535)
1f	+5.6 (531)
2a	+4.0 (525)
2b	+6.6 (517)
3a	+3.8 (525)
3b	+7.9 (524)
4a	+5.5 (527)
4b	−0.7 (527)
5	+1.7 (524)

[a] Data collected from Ref. [33].

The visible ECD spectra of *helico*BODIPYs **1a**, **1c**, **1e**, **4a** and **4b** (*R,R*, enantiomers were computed) were theoretically simulated (TD PCM/CAM-B3LYP/6-311G*) in chloroform. These dyes were selected for comparison purposes (*e.g.*, note in Table 2 the higher absolute g_{abs} value of **1c** when compared to related, seminal **1a**, or the g_{abs} sign reversal of **4b** when compared to related **4a**). The simulation supports both the observed visible couplets, including their Cotton effects, and the differences found in the reached absolute visible maximum g_{abs} values. Thus, these simulations predict visible ECD couplets with negative Cotton effect for all the computed *R,R* enantiomers at their corresponding more stable conformation, with the exception of **4b**, for which a positive visible ECD couplet is predicted, in agreement with the found ECD reversal for this dye (see Fig. S13 in ESI). Moreover, the theoretical absolute visible maximum g_{abs} values, $|g_{cal}|$, calculated from the corresponding computed $|\mu|$, $|m|$ and θ values (see Fig. S14 and Table S4 in ESI) correlate well with the experimental ones ($|g_{abs}|$), being of similar order of magnitude. Noteworthy, the conducted computation reveals that, for these *helico*BODIPYs, high $|g_{abs}|$ values are not always associated with high $|m|$ values, nor with low $|\mu|$ ones (note in Table S4 in ESI that the computed $|\mu|$ values are similar), but to a proper combination of

$|m|$ and θ values, which are tuned by selecting the involved bridge. In this context, the possibility of tuning θ values to modulate the dichroic factors is an interesting capability of the flexible *helico*BODIPYs. Note that most of the optically active SOMs are conformationally rigid. Therefore, the modulation and optimization of their chiroptical efficiency (*g* values) can be only done by acting on the transition probability (*i.e.*, by changing the relative magnitudes of the transition dipole moments, $|\mu|$ and $|m|$), with the consequent decrease of the transition probability. However, in the herein reported flexible *helico*BODIPYs the computational simulation reveals that the mutual orientation of the dipole moments (θ) has a pivotal role in the g_{abs} value. Such disposition can be easily modulated by accessible structural modifications at the involved flexible bridge directed towards optimizing the g_{abs} value without significantly decreasing the transition probability.

The computation of the g_{abs} and the ECD signatures of *helico*BODIPYs **4a** and **4b**, bearing cyclic bridges, is more challenging, since their molecular geometries evolve from an extended helix to a pleated arrangement (see Fig. S10 in ESI), where the BODIPY units can adopt different dispositions during the geometry optimization. To shed light on the influence of such BODIPY dispositions on the ECD signatures, we carried out a study of the preferred conformations of *R,R* **4a** and **4b**, in terms of their relative energy, the mutual orientation of their BODIPY units, and the visible ECD spectrum predicted from each of them. Thus, for both dyes the more stable conformations correspond to a typical chair-like conformation for the cyclohexane-based bridge with two equatorial substituents, but differing in the mutual orientation of the pendant BODIPY units. Thus, in both dyes, **4a** and **4b**, the two most stable conformers (**I** and **II**; separated by just 2 kcal mol^{-1}; see Fig. S15 in ESI) have the fluorine atoms of a one of the BODIPY units facing the closest *N*-hydrogen (or *N*-methyl) group of the bridge. However, whereas in **I** the second BODIPY unit holds this arrangement, in **II** the second BODIPY rotates 180°, its fluorine atoms facing now the closest cyclohexane methyne hydrogen (see Fig. S12 in ESI). The stability of these energetically-close conformers reverses depending on the substitution of the involved bridge nitrogens. Thus, for **4a**, bearing protic amino groups (NH), conformer **I** is the most stable, likely due to hydrogen bonding interactions between the BODIPY fluorines and the hydrogen at the bridge amino groups (see **I** Fig. S15 in ESI). The predicted visible negative Cotton effect from this conformer agrees with the experimental one (positive for *S,S-helico*BODIPY **4a**; it must be remarked here that computations were done with the *R,R* enantiomer). However, *N*-methylation of the bridge amino groups (**4b**) preferably stabilizes conformer **II**, likely owing to steric reasons (see **II** in Fig. S15 in ESI). The predicted ECD spectrum displays the opposite Cotton effect (see Fig. S13 in ESI), in agreement with the couplet reversal experimentally detected for **4b** when compared to **4a** (see Fig. 9B). Therefore, properly selecting the bridge of the *helico*BODIPY not only allows a fine modulation of the strength of its ECD visible signal (magnitude of the maximum visible g_{abs} value), but also the control of its sign (sign of maximum visible g_{abs} value).

4. Conclusions

It is demonstrated, by computationally-aided spectroscopic characterization, that the photophysical and chiroptical (ECD) visible signatures of the highly-accessible and -variable *helico*BODIPY dyes are ruled by a characteristic BODIPY-to-BODIPY CT enabled by the SBCT mechanism. This CT can be finely modulated by adjusting the sterical overcrowding at the bridge, which is easily done by workable chemistry. Thus, increasing this overcrowding, by using bridge building blocks involving bulky substituents, elongates the *helico*BODIPY molecular helix, and places the BODIPY units in a more orthogonal disposition to each other, which promotes SBCT. In fact, in specific overcrowded cases and experimental conditions, it is possible to detect a dual visible absorption (non-common short-wavelength CT absorption plus the LE one) and/or a dual visible emission (non-common long-wavelength CT emission plus the LE one). Interestingly, enhanced participation of the forbidden CT transition enables a marked enhancement of the observed visible ECD couplet, as measured by the corresponding maximum visible g_{abs} values. Thus, there is a reliable correlation between the participation of CT absorption and the capability of the molecular dye to differentially absorb circularly polarized light. Thus, the higher the short-wavelength visible CT absorption, the higher the intensity of the ECD visible signal. In this context, the reported results support that properly increasing the probability of forbidden CT transitions, by easily modifying the molecular structure, arises as a suitable tool to ameliorate and modulate the ECD response of CP-active SOMs with helically-flexible chirality, as the *helico*BODIPYs are. Interestingly, the Cotton effect of a given *helico*BODIPY enantiomer based on cyclohexane-1,2-diamine bridge can be easily reversed by workable N-methylation, the latter triggering the rotation of one of the involved BODIPY units, as supported computationally. Further work is in progress to ascertain whether this approach to modulate the ECD signatures can also be extended to modulate the CPL ones, in particular valuable CPL brightness, and thereby to establish an easy guide to develop efficient and sign-tunable CPL-SOMs on the basis of using accessible and conformational flexible multichromophoric organic dyes with helical chirality.

CRediT authorship contribution statement

Carolina Díaz-Norambuena: Investigation. **Cesar Ray:** Investigation. **Teresa Arbeloa:** Investigation. **Ainhoa Oliden-Sánchez:** Investigation. **Florencio Moreno:** Formal analysis, Methodology. **Beatriz L. Maroto:** Formal analysis, Methodology. **Jorge Bañuelos:** Conceptualization, Funding acquisition, Supervision, Writing – original draft, Writing – review & editing. **Santiago de la Moya:** Conceptualization, Funding acquisition, Supervision, Writing – original draft, Writing – review & editing.

Declaration of competing interest

The authors declare that they have no known competing financial interests or personal relationships that could have appeared to influence the work reported in this paper.

Data availability

Data will be made available on request.

Acknowledgements

This research received financial support by the Spanish Ministerio de Ciencia e Innovación (MCIN)/Agencia Estatal de Investigación (AEI) Grants: PID2020-114755 GB-C32 and -C33 funded by MCIN/AEI/10.13039/501100011033. Gobierno Vasco (IT1639-22) is also thanked for financial support. C.D.-N. thanks MICIN for a FPI contract.

Appendix A. Supplementary data

Supplementary data to this article can be found online at https://doi.org/10.1016/j.dyepig.2023.111907.

References

[1] Wang Y, Xu J, Wang Y, Chen H. Emerging chirality in nanoscience. Chem Soc Rev 2013;42:2930–62. https://doi.org/10.1039/C2CS35332F.
[2] Han J, Guo S, Lu H, Liu S, Zhao Q, Huang W. Recent progress on circularly polarized luminescent materials for organic optoelectronic devices. Adv Opt Mater 2018;1800538. https://doi.org/10.1002/adom.201800538.
[3] Kumar J, Nakashima T. Circularly polarized luminescence in chiral molecules and supramolecular assemblies. J Phys Chem Lett 2015;6:3445–52. https://doi.org/10.1021/acs.jpclett.5b01452.

[4] Chen N, Yan B. Recent theoretical and experimental progress in circularly polarized luminescence of small organic molecules. Molecules 2018;23:3376. https://doi.org/10.3390/molecules23123376.

[5] Tanaka H, Inoue Y, Mori T. Circularly polarized luminescence and circular dichroisms in small organic molecules: correlation between excitation and emission dissymetry factors. ChemPhotoChem 2018;2:386–402. https://doi.org/10.1002/cptc.201800015.

[6] Chen Y. Circularly polarized luminescence based on small organic fluorophores. Mater Today Chem 2022;23:100651. https://doi.org/10.1016/j.mtchem.2021.100651.

[7] Sánchez-Carnerero EM, Agarrabeitia AR, Moreno F, Maroto BL, Muller S, Ortiz MJ, de la Moya S. Circularly polarized luminescence from simple organic molecules. Chem Eur J 2015;21:13488–500. https://doi.org/10.1002/chem.201501178.

[8] Ma JL, Peng Q, Zhao CH. Circularly polarized luminescence switching in small organic molecules. Chem Eur J 2019;25:15441–54. https://doi.org/10.1002/chem.201903252.

[9] Brunel JM. BINOL: a versatile chiral reagent. Chem Rev 2005;105:857–97. https://doi.org/10.1021/cr0500479.

[10] Wan SP, Lu HY, Li M, Chen CF. Advances in circularly polarized luminescence materials based on axially chiral compounds. J Photochem Photobiol, C 2022;50:100500. https://doi.org/10.1016/j.jphotochemrev.2022.100500.

[11] Xu Y, Ni Z, Xiao Y, Chen Z, Wang S, Gai L, Zheng YX, Shen Z, Lu H, Guo Z. Helical β-isoindigo-Based chromophores with B-O-B bridge: Facile synthesis and tunable near-infrared circularly polarized luminescence. Angew Chem Int Ed 2023;62:e202218023. https://doi.org/10.1002/anie.202218023.

[12] Arrico F, Di Bari L, Zinna F. Quantifying the overall efficiency of circularly polarized emitters. Chem Eur J 2021;27:2920–34. https://doi.org/10.1002/chem.202002791.

[13] Lin WB, He DQ, Lu HY, Hu ZQ, Chen CF. Sign inversions of circularly polarized luminescence for helical compounds by chemically fine-tuning operations. Chem Commun 2020;56:1863–6. https://doi.org/10.1039/C9CC08573D.

[14] Takaishi K, Murakami S, Iwachido K, Ema T. Chiral exciplex dyes showing circularly polarized luminescence: extension of the excimer chirality rule. Chem Sci 2021:14570–6. https://doi.org/10.1039/D1SC04403F.

[15] Greenfield J, Wade J, Brandt JR, Shi X, Penfold TJ, Fuchter MJ. Pathways to increase the dissimetry in the interaction of chiral light and chiral molecules. Chem Sci 2021;12:8589–602. https://doi.org/10.1039/D1SC02335G.

[16] Chen JF, Gao QX, Liu L, Chen P, Wei TB. A pillar[5]arene-based planar chiral charge-transfer dye with enhanced circularly polarized luminescence and multiple responsive chiroptical changes. Chem Sci 2023;14:987–93. https://doi.org/10.1039/D2SC06000K.

[17] Chen XY, Li JK, Zhao WL, Du CZ, Li M, Chen CF, Wang XY. Amplification of dissymmetry factors by dihedral angle engineering in donor-acceptor type circularly polarized luminescence materials. J Mater Chem C 2023;11:893–7. https://doi.org/10.1039/D2TC04848E.

[18] Nagata Y, Mori T. Irreverent nature of dissymmetry factor and quantum yield in circularly polarized luminescence of small organic molecules. Front Chem 2020;8:448. https://doi.org/10.3389/fchem.2020.00448.

[19] Lu H, Mack J, Nyokong T, Kobayashi N, Shen Z. Optically active BODIPYs. Coord Chem Rev 2016;318:1–15. https://doi.org/10.1016/j.ccr.2016.03.015.

[20] Bañuelos J. BODIPY dye, the most versatile fluorophore ever? Chem Rec 2016;16:335–48. https://doi.org/10.1002/tcr.201500238.

[21] Boens N, Verbelen B, Ortiz MJ, Jiao L, Dehaen W. Synthesis of BODIPY dyes through postfunctionalization of the boron dipyrromethene core. Coord Chem Rev 2019;399:213024. https://doi.org/10.1016/j.ccr.2019.213024.

[22] Sánchez-Carnerero EM, Moreno F, Maroto BL, Agarrabeitia AR, Ortiz MJ, Vo BG, Muller G, de la Moya S. Circularly polarized luminescence by visible-light absorption in a chiral O-BODIPY dye: unprecedented design of CPL organic molecules from achiral chromophores. J Am Chem Soc 2014;136:3346–9. https://doi.org/10.1021/ja412294s.

[23] Wu Y, Wang S, Li Z, Lu H. Chiral binaphthyl-linked BODIPY analogues: synthesis and spectroscopic properties. J Mater Chem C 2016;4:4668–74. https://doi.org/10.1039/C6TC00975A.

[24] Maeda C, Suka K, Nagahata K, Takaishi K, Ema T. Synthesis and chiroptical properties of chiral carbazole-based BODIPYs. Chem Eur J 2020;26:4261–8. https://doi.org/10.1002/chem.202081963.

[25] Sakai H, Suzuki Y, Tsurui M, Kitagawa Y, Nakashima Y, Kawai T, Kondo Y, Matsuba G, Hasegawa Y, Hasobe T. Controlled molecular assemblies of chiral boron dipyrromethene derivatives for circularly polarized luminescence in the red and near-infrared regions. J Mater Chem C 2023;11:2889–96. https://doi.org/10.1039/D2TC05006D.

[26] Kolemen S, Cakmak Y, Kostereli Z, Akkaya EU. Atropoisomeric dyes: axial chirality in orthogonal BODIPY oligomers. Org Lett 2014;16:660–3. https://doi.org/10.1021/ol403193f.

[27] Zina F, Bruhn T, Guido CA, Ahrens J, Bröring M, Di Bari L, Pescitelli G. Circularly polarized luminescence from axially chiral BODIPY DYEmers: an experimental and computational study. Chem Eur J 2016;22:16089–98. https://doi.org/10.1002/chem.201602684.

[28] Maeda C, Nagahata K, Shirakawa T, Ema T. Azahelicene-fused BODIPY analogues showing circularly polarized luminescence. Angew Chem Int Ed 2020;59:7813–7. https://doi.org/10.1002/anie.202001186.

[29] Sánchez-Carnerero EM, Moreno F, Maroto BL, Agarrabeitia AR, Bañuelos J, Arbeloa T, López-Arbeloa I, Ortiz MJ, de la Moya S. Unprecedented induced axial chirality in a molecular BODIPY dye: strongly bisignated electronic circular dichroism in the visible region. Chem Commun 2013;49:11641–3. https://doi.org/10.1039/C3CC47570K.

[30] Ray C, Sánchez-Carnerero EM, Moreno F, Maroto BL, Agarrabeitia AR, Ortiz MJ, López-Arbeloa I, Bañuelos J, Cohovi KD, Lunkley JL, Muller G, de la Moya S. Bis(haloBODIPYs) with labile helicity: valuable simple organic molecules that enable circularly polarized luminescence. Chem Eur J 2016;22:8805–8. https://doi.org/10.1002/chem.201601463.

[31] Berova N, Di Bari L, Pescitelli G. Application of electronic circular dichroism in configurational and conformational analysis of organic compounds. Chem Soc Rev 2007;36:914–31. https://doi.org/10.1039/B515476F.

[32] Jiménez J, Moreno F, Maroto BL, Cabreros TA, Huy AS, Muller G, Bañuelos J, de la Moya S. Modulating ICT emission: a new strategy to manipulate the CPL sign in chiral emitters. Chem Commun 2019;5:1631–4. https://doi.org/10.1039/C8CC09401B.

[33] Ray C, Díaz-Norambuena C, Johnson M, Moreno F, Maroto BL, Bañuelos J, Muller G, de la Moya S. Tuning CPL by helical pitch modulation in helically flexible small organic multichromophores. J Mater Chem C 2023;11:456–61. https://doi.org/10.1039/D2TC04793D.

[34] Kellogg M, Akil A, Ravinson DSM, Estergreen L, Bradforth SE, Thompson ME. Symmetry breaking charge transfer as a means to study electron transfer with no driving force. Faraday Discuss 2019;216:379–94. https://doi.org/10.1039/C8FD00201K.

[35] Liu Y, Zhao J, Iagatti A, Bussotti L, Foggi P, Castellucci E, Di Donato M, Han KL. A revisit to the orthogonal bodipy dimers: experimental evidence for the symmetry breaking charge transfer-induced intersystem crossing. J Phys Chem C 2018;122:2502–11. https://doi.org/10.1021/acs.jpcc.7b10213.

[36] Estergreen L, Mencke AR, Cotton DE, Korovina NV, Michl J, Roberts ST, Thompson ME, Bradforth SE. Controlling symmetry breaking charge transfer in BODIPY pairs. Acc Chem Res 2022;55:1561–72. https://doi.org/10.1021/acs.accounts.2c00044.

[37] Quin W, Rohand T, Baruah M, Stefan A, Van der Auweraer M, Dehaen W, Boens N. Solvent-dependent photophysical properties of borondipyrromethene dyes in solution. Chem Phys Lett 2006;420:562–8. https://doi.org/10.1016/j.cplett.2005.12.098.

[38] Vasiuta R, Plenio H. Observing initial steps in gold-catalyzed alkyne transformations by utilizing BODIPY-tagged phosphine-gold complexes. Chem Eur J 2016;22:6353–60. https://doi.org/10.1002/chem.201600264.

[39] Qin W, Leen V, Rohand T, Dehaen W, Dedecker P, Van der Auweraer M, Robeyns K, Van Meervelt L, Beljonne D, Van Averbeke B, Clifford JN, Driesen K, Binnemans K, Boens N. Synthesis, spectroscopy, crystal structure, electrochemistry, and quantum chemical and molecular dynamics calculation of a 3-anilino difluoroboron dipyrromethene dye. J Phys Chem A 2009;113:439–47. https://doi.org/10.1021/jp8077584.

[40] Volkova YA, Brizet B, Harvey PD, Averin AD, Goze C, Denat F. BODIPY dyes functionalized with pendant cyclic and acyclic polyamines. Eur J Org Chem 2013:4270–9. https://doi.org/10.1002/ejoc.201300414.

[41] Knight JG, Alnoman RB, Wadell PG. Synthesis of 3-aminoBODIPY dyes via copper-catalyzed vicarious nucleophilic substitution of 2-halogeno derivatives. Org Biomol Chem 2015;13:3819–29. https://doi.org/10.1039/C4OB02626H.

[42] Ripoll C, Cheng C, García-Fernández E, Li J, Orte A, Do H, Jiao L, Robinson D, Crovetto L, González-Vera JA, Talavera EM, Álvarez-Pez JM, Boens N, Ruedas-Rama MJ. Synthesis and spectroscopy of benzylamine-substituted BODIPYs for bioimaging. Eur J Org Chem 2018:2561–71. https://doi.org/10.1002/ejoc.201800083.

[43] Alnoman RB, Stachelek P, Knight JG, Harriman A, Wadell PG. Synthesis of 2-aminoBODIPYs by palladium catalysed amination. Org Biomol Chem 2017;15:7643–53. https://doi.org/10.1039/C7OB01767G.

[44] Nepomnyashchii AB, Bard AJ. Electrochemistry and electrogenerated chemiluminescence of BODIPY dyes. Acc Chem Res 2012;45:1844–53. https://doi.org/10.1021/ar200278b.

[45] Benniston AC, Clift S, Hagon J, Lemmetyinen H, Tkachenko NV, Clegg W, Harrington RW. Effect on charge transfer and charge recombination by insertion of a naphthalene-based bridge in molecular dyads based on borondipyrromethene (Bodipy). ChemPhysChem 2012;13:3672–81. https://doi.org/10.1002/cphc.201200510.

[46] Nano Ziessel R, Stachelek P, Harriman A. Charge-recombination fluorescence form push-pull electronic systems constructed around amino-substituted styryl-BODIPY dyes. Chem Eur J 2013;19:13528–37. https://doi.org/10.1002/chem.201301045.

[47] Forde Freixas VM, Fernández-Alberti S, Neukirch AJ, Tretiak S. Charge-transfer luminescence in a molecular donor-acceptor complex: computational insights. J Phys Chem Lett 2022;13:8755–60. https://doi.org/10.1021/acs.jpclett.2c02479.